C. R. Physique 15 (2014) 527–535

Contents lists available at ScienceDirect

Comptes Rendus Physique

www.sciencedirect.com

Prix Aniuta Winter-Klein 2013 de l'Académie des sciences

Is glass brittle at all scales?

Le verre est-il fragile à toutes les échelles ?

Élisabeth Bouchaud [a,b,*]

[a] *CEA-Saclay, L'Orme des Merisiers, DSM/IRAMIS/SPEC, 91191 Gif-sur-Yvette cedex, France*
[b] *PSL Research University, ESPCI–ParisTech, UMR Gulliver 7083, EC2M, 10 rue Vauquelin, 75005 Paris, France*

ARTICLE INFO

Article history:
Available online 3 July 2014

Keywords:
Stress corrosion cracking
Quasi-brittle fracture
Damage
Silicate glass

Mots-clés :
Corrosion sous contrainte
Rupture quasi fragile
Endommagement
Verre de silice

ABSTRACT

Although silicate glass is considered as the archetype of brittle materials, which break without deforming irreversibly, its fracture involves some dissipation. By examining the *post-mortem* fracture surfaces, by following *in situ* the progression of a stress corrosion crack and by measuring the depth of penetration of water in the material during slow fracture, we show that glass behaves in fact in a quasi-brittle manner, with a damaged zone of ∼10 nm developing ahead of the crack tip.

RÉSUMÉ

Bien que le verre de silice soit considéré comme l'archétype des matériaux fragiles, qui cassent sans se déformer, sa rupture s'accompagne de dissipation. Par l'examen *post-mortem* de surfaces de rupture, le suivi *in situ* de la progression d'une fissure de corrosion sous contrainte et la mesure de la profondeur de pénétration de l'eau dans le matériau pendant sa fissuration lente, nous montrons que le verre se comporte en fait de manière quasi fragile, avec une zone endommagée d'une dizaine de nanomètres qui se développe en pointe de fissure.

1. Introduction

Silicate glasses are usually considered as the archetype of brittle materials, which break without deforming prior to fracture. As a consequence, no energy dissipation is expected to take place during fracture, and Griffith's energy balance criterion [1,2] should be perfectly fulfilled: the stored elastic energy should exactly compensate for the creation of two free surfaces. Let us remark that if this is the physical definition of "brittleness", then the cleavage of perfect crystals is indeed brittle. As a matter of fact, in a perfect crystal, all the atomic bonds having identical energies, the first one to break is the one located exactly at the crack tip, where the stress is the largest. Cleavage thus proceeds by successive openings of atomic bonds at the crack tip, and the fracture energy is exactly equal to the product of the number of cut bonds by their energy. Cleavage surfaces are also perfectly flat, and used for that quality in surface science experiments.

* Correspondence to: PSL Research University, ESPCI–ParisTech, UMR Gulliver 7083, EC2M, 10 rue Vauquelin, 75005 Paris, France.
E-mail address: elisabeth.bouchaud@espci.fr.

http://dx.doi.org/10.1016/j.crhy.2014.06.002
1631-0705/

If one considers now an amorphous material such as glass, the balance is not as simple. Some bonds may require less energy to be broken, and, in consequence, they may break first even if they are located somewhat away from the crack tip. Furthermore, the orientation of the bond at the crack tip may not be adequate: if the bond is perpendicular to the direction of the applied tension, it undergoes a much smaller tension than in the case when it is parallel to it. Knowing that the only bonds that can be broken are the Si–O bonds linking together silica tetrahedra, and knowing their energy, 110 kcal/mol [3], one can estimate the energy needed to break all the Si–O bonds per unit area to be 2 $\mathrm{J\,m^{-2}}$. It can be compared to the fracture energy, $\simeq K_{\mathrm{Ic}}^2/E \simeq 9\ \mathrm{J\,m^{-2}}$, where $K_{\mathrm{Ic}} \simeq 0.8\ \mathrm{MPa\,m^{-1/2}}$ and $E \simeq 70$ GPa are respectively the fracture toughness and the Young modulus of silica. In a humid environment, as recalled in the following, a crack propagates at a lower stress intensity factor, depending on the humidity rate. Typically, propagation was observed to take place at a velocity $v \simeq 10^{-11}\ \mathrm{m\,s^{-1}}$ for a stress intensity factor $\simeq 0.4\ \mathrm{MPa\,m^{-1/2}}$ at 40% humidity [4]. Even in this case, the fracture energy is $\simeq 4.5\ \mathrm{J\,m^{-2}}$, a value more than twice as higher as the expected one. Since glass is deprived of plasticity when loaded in tension—the plastic zone size can be estimated to be of the order of $R_{\mathrm{c}} = \pi/8(K_{Ic}/\sigma_{\mathrm{Y}})^2 \simeq 1.7$ nm [2] (σ_{Y} being the yield stress)—the central question is the nature of the dissipated energy.

The only possibility seems to be a quasi-brittle damage spreading similar to the one that can be observed at a macroscopic scale in materials that are highly disordered, such as wood, concrete, or paper, for example [5]. This is indeed what is suggested by Molecular Dynamics (MD) simulations for other amorphous materials [6,7] and for silica [8], independently of the interaction potential used [9].

We have performed three kinds of experiments in order to track quasi-brittle damage in glass. We have first examined the morphology of glass fracture surfaces, and compared it to observations performed on other materials [10]. These experiments are discussed in Section 2. We have also observed damage spreading around a crack tip during its propagation, using an Atomic Force Microscope (AFM) [11–13]. Because scanning with an AFM takes time, we were constrained to follow very slow propagating cracks. This cannot be achieved in UHV conditions, this is why we have decided to follow stress corrosion cracks [2]. Under very moderate external tensile stresses, corresponding to stress intensity factors K_{I} lower than K_{Ic}, cracks may indeed grow in silicate glasses, thanks to the hydrolysis of the Si–O bonds, a chemical reaction that involves the water molecules of the surrounding environment. This is a complex phenomenon, which started to be studied in the 1960s [14,15] and is not yet fully understood (see [16] for a review). In the classical picture, proposed first by Michalske and Bunker [17], water molecules break the Si–O bonds located exactly at the crack tip. For small enough external loads, the crack velocity is controlled by the rate of the chemical reaction, which depends both on the degree of ambient humidity and on the applied stress. It is in this regime, traditionally referred to as "Stage I" [14,2], that our AFM experiments have been performed. We report on them in Section 3. However, as we will discuss later, our AFM observations are confined to the external surface of the specimens, which are immersed in an infinite reservoir of water molecules. In order to explore damage spreading within the bulk, we decided to track the water molecules that had penetrated into the material during crack propagation: where there is water, there are broken Si–O bonds, which constitute damage in our case. For that purpose, we have measured the neutron reflectivity of fracture surfaces, and shown that it is modified by water trapped under the surface [18,19]. These experiments are discussed in Section 4. Finally, Section 5 is devoted to a general discussion, leading to open questions.

2. Morphology of glass fracture surfaces

Since 1984 and the pioneering experiment by B. Mandelbrot and collaborators [20], the quantitative study of materials fracture surfaces has inspired a lot of research. In 1990, we conjectured that, contrary to the common belief, the roughness or Hurst exponent characterizing the morphology of these surfaces was *universal* [21], i.e. independent of both the material and the loading. This simple picture has evolved since then [5], but the idea of "universality classes" has persisted. In fact, it was shown that the structure of fracture surfaces is a signature of the presence of damage. In all cases, fracture surfaces are anisotropic self-affine surfaces, characterized by a roughness index ζ in a direction perpendicular to the direction of crack propagation, and by a roughness exponent $\beta \neq \zeta$ in the direction of crack propagation [22]. The two classes of universality correspond to [23] (i) purely brittle fracture of disordered materials for which $\zeta \simeq 0.4$ and $\beta \simeq 0.5$, (ii) quasi-brittle or ductile fracture, for which $\zeta \simeq 0.75$ and $\beta \simeq 0.6$. In all cases, however, height correlations have the same Family–Vicsek type of structure [5], i.e.:

$$\Delta h(\Delta x, \Delta z) \equiv \left\langle \left(y(x_{\mathrm{A}} + \Delta x, z_{\mathrm{A}} + \Delta z) - y(x_{\mathrm{A}}, z_{\mathrm{A}}) \right)^2 \right\rangle_{x_{\mathrm{A}}, z_{\mathrm{A}}}^{1/2} = \Delta x^{\beta} f\left(\frac{\Delta z}{\Delta x^{1/\kappa}} \right) \tag{1}$$

where $\Delta h(\Delta x, \Delta z)$ is the mean height difference between points of the fracture surface separated by a distance Δx along the direction of crack propagation and by a distance Δz in the perpendicular direction (see Fig. 1).

The so-called "dynamic exponent" κ is simply the ratio of the roughness indices ζ and β: $\kappa = \zeta/\beta$.

Fig. 2 shows the results obtained for pure silica, broken in stress corrosion conditions, i.e. at a humidity rate of ∼40%. In Fig. 2 (left), the two one-dimensional correlation functions measured along perpendicular and parallel directions allow us to determine roughness exponents $\zeta \simeq 0.75$ and $\beta = 0.6$, respectively. These are the exponents used to rescale the curves shown in Fig. 2 (right) onto a single master curve, by plotting $\Delta h(\Delta x, \Delta z)/\Delta x^{\beta}$ against $\Delta z/\Delta x^{1/\kappa}$, which corresponds to expression (1). Any other choice of exponents fails to provide a satisfactory collapse.

Let us notice that both in the parallel and perpendicular directions, the correlation length (i.e. the upper limit of the observed scaling domains) is of the order of $\simeq$ 20 nm. Although these are scales much smaller than the ones involved

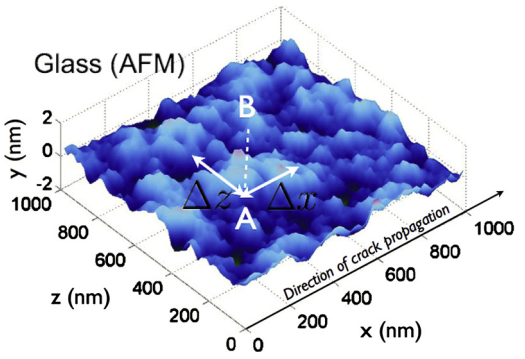

Fig. 1. (Color online.) Glass fracture surface observed in Atomic Force Microscopy. In order to compute the structure function $\Delta h(\Delta x, \Delta z)$, one measures the height difference between points A and B distant by Δx along the direction of crack propagation x and by Δz along the perpendicular direction z. This quantity is averaged over all points A belonging to the fracture surface.

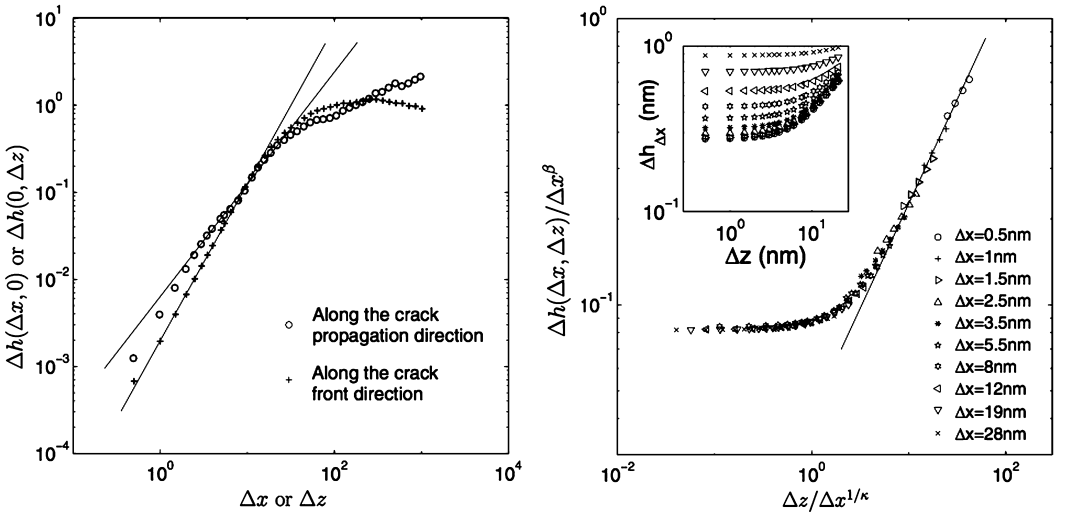

Fig. 2. *Left.* Height correlation functions measured along profiles parallel and perpendicular to the direction of crack propagation (Δx and Δz are both expressed in nanometers). Exponents determined this way are: $\beta \simeq 0.6$ and $\zeta \simeq 0.75$. *Right.* 2D height correlation function: $\Delta h(\Delta x, \Delta z)/\Delta x^{\beta}$ is plotted against $\Delta z/\Delta x^{1/\kappa}$, which corresponds to expression (1). The exponents which allow for a collapse of all the curves onto a single master curve are $\beta \simeq 0.6$ and $\zeta \simeq 0.75$. $\kappa = \zeta/\beta \simeq 1.2$.

in wood or concrete fracture, or even in paper tearing, these exponents are extremely close to the ones characteristic of quasi-brittle failure. The measured value $\zeta \simeq 0.75$ in particular, seems to exclude the 0.4 value expected for purely brittle fracture. These results are fairly robust: they do not depend on the humidity rate—which we could control between 20 and 70%—, the crack velocity that varied between 10^{-11} and 10^{-5} m s^{-1}, and even the nature of the silicate glass: beyond pure silica [13,22], we studied window glass [10,24], and more or less devitrified vitroceramics [11,4,12].

However, we have also realized that small-scale quantitative measurements of this kind are doubtful because of tip effects [25]. Actually, if the tip has large radius of curvature, it may smooth out the real profile $y(x)$ into a profile $\tilde{y}$ which has a larger roughness index (see Fig. 3). A profile with a roughness index $\zeta = 0.4$ may be interpreted wrongly as a profile with exponent $\zeta = 0.75$ because of this artifact. Of course, $\beta = 0.5$ has no reason to appear as $\beta = 0.6$ in experiments where scanning is performed along the direction of crack propagation. Furthermore, it is unlikely that the structure of the modified surface $\tilde{y}(x, z)$ is also of the Family–Vicsek type, which is expected for a real fracture surface, whether there is damage or not. This, however, would require further simulations.

As we will see, *in situ* AFM studies are also limited in resolution but in a slightly different way.

3. *In situ* observations of damage around a stress corrosion crack tip

We have explored stress corrosion cracking in two types of silicate glasses: pure silica and alumino silicates with lithium. In order to be able to scan a region of $\sim 100 \times 100$ nm^2, which takes about one minute, we have to limit crack velocity to values smaller than $\sim$100 nm in $\sim$60 s, i.e. ~ 1 nm s^{-1} to avoid a complete failure of the observation zone before scanning is over. This is why, for these experiments, we had to control very carefully the propagation speed. For that purpose, we used a stable specimen geometry commonly used to fracture brittle materials, double cleavage drilled compression (DCDC)

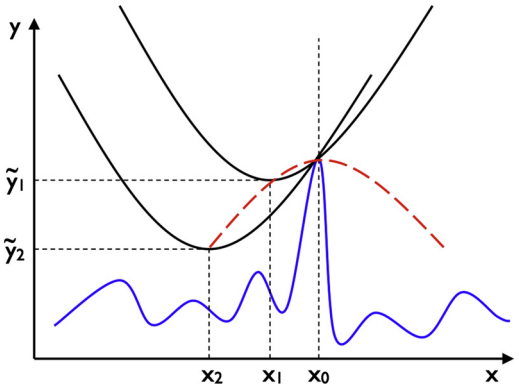

Fig. 3. (Color online.) Sketch explaining the effect of a large radius of curvature at the AFM tip. For two closeby points, the probe (depicted here as a parabola in black solid line) touches a unique distant peak on the profile. We have drawn the corresponding portion of the actually measured profile, $\tilde{y}$ (red dotted line). Obviously, the roughness of $\tilde{y}$ is less than the one of y, and its roughness index will hence be larger.

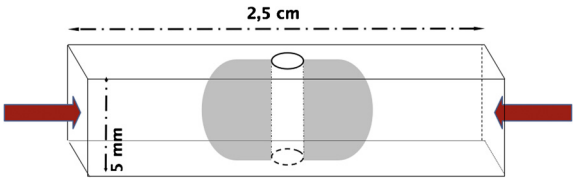

Fig. 4. Sketch of the DCDC specimens used. The hole has a radius $a = 0.5$ mm. Samples are loaded through uniaxial compression. The two symmetric cracks that emerge from the central hole are locally submitted to tension, due to the Poisson effect. We follow one of these cracks with an AFM tip.

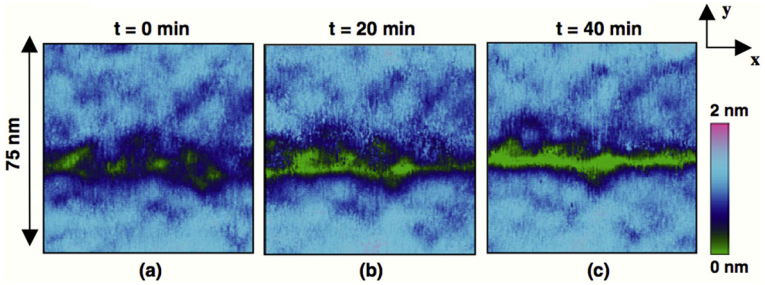

Fig. 5. Sequence of successive topographic AFM frames showing a crack propagating at the surface of an alumino-silicate glass with lithium. The scan size is 75×75 nm^2, and the measured heights range over 2 nm. The recording time for one frame is around 3 min, and two successive frames are separated by 20 min. The crack front propagates from the left to the right (x-direction) with a mean velocity V of around 10^{-11} m s^{-1}. (a) Evidence of nanometric-scale damage ahead of the main crack front, (b) damage growth, (c) failure of the observed zone of the sample.

samples (see [26,4] for details) to which a compressive stress is applied. By the Poisson effect, this compressive external load results in a tensile opening stress acting on the two symmetric cracks that emerge from the central hole of radius a (see Fig. 4).

The external compressive stress σ_0 is gradually increased by the slow constant displacement (0.02 mm min^{-1}) of the jaws of the loading machine. Once the two symmetric cracks are initiated, the displacement of the jaws is stopped. The crack front then propagates at a stress intensity factor K_I which decreases with the crack length c as $K_I = \sigma_0\sqrt{a}/(0.375\,c/a + 2)$. At a given value of K_I corresponds a unique value of the crack velocity V. Typically, depending on the glass composition—and on its more or less devitrified nature—, values of V ranging from 10^{-11} to 10^{-9} m s^{-1} are obtained for K_I varying between 0.4 and 0.5 N m$^{1/2}$.

One of the two cracks is followed by AFM during its propagation. Note that the surface that is explored is polished until an RMS roughness of ∼0.25 nm for a 10×10-μm^2 scan size is reached.

In all cases, one observes depressions (in green in Fig. 5, while the flat mean surface appears in blue), which we have interpreted as quasi-brittle damage preceding the main crack. Note however that, because of the poor lateral resolution of an AFM (∼5 nm), it is impossible to deduce from these observations the extent of the damaged zone.

Mostly for this reason, our conclusions were questioned [27,28], and, by determining the local stress intensity factor by using digital image correlation techniques applied to AFM frames, other authors concluded that there is no departure from elasticity at distances larger or equal than ∼10 nm (resolution of their experiments) from the crack tip [29]. Hence a more accurate technique had to be used in order to understand whether failure in glass is indeed preceded by damage

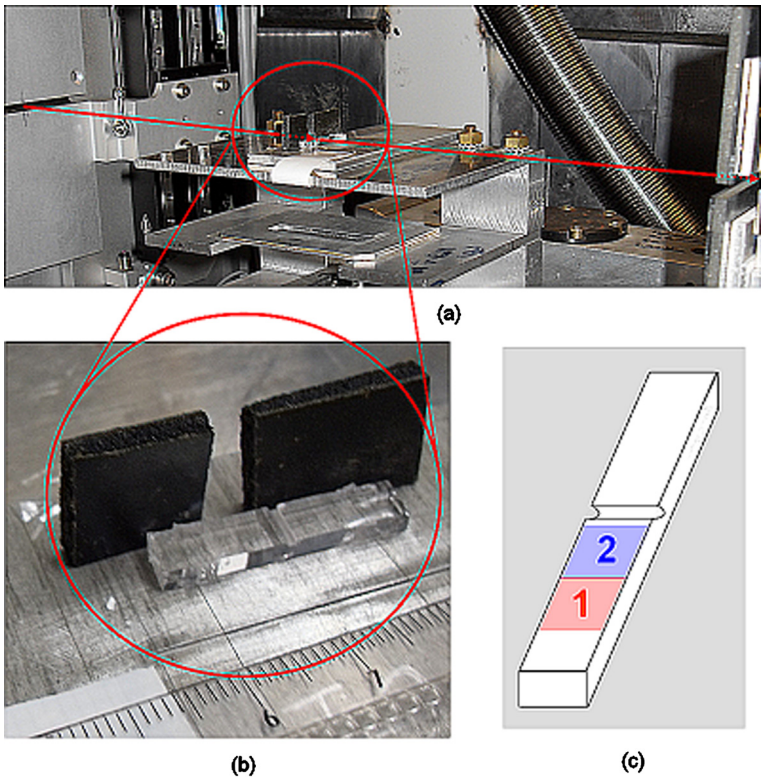

Fig. 6. (Color online.) (a) Photograph of the experimental setup. The neutron beam is schematized in red, incoming from the last slit of the collimator, reflecting on the sample and going within the slit in front of the detector. (b) Drawing of the broken sample, showing the two black sheets of B_4C used to select one area of interest (see text). (c) Sketch of the broken sample, with zone (1) corresponding to an average velocity of 10^{-8} m s^{-1} and zone (2) corresponds an average velocity of 10^{-6} m s^{-1}.

at very small scales. As we shall see in the following section, neutron reflection indeed provides the required sensitivity. It also allows us to probe the bulk of the specimen, which is unaccessible to AFM. As a matter of fact, stresses at the surface of the specimen—where plane stress conditions apply—are different from the ones in volume–plane strain conditions. But, much more importantly, the surface is in contact with an infinite reservoir of water molecules. On the contrary, water has to diffuse within the bulk in order to provoke damage.

4. Water stored around the crack tip

Let us consider the diffusion coefficient of water in silica, in order to estimate the plausibility of this scenario. Although experiments have been performed at high temperature only [30,31], a rough extrapolation of Tomozawa et al.'s results [32] suggests a water diffusion coefficient in silica of the order of $\sim 10^{-21}$ cm^2 s^{-1} at room temperature. This means that the penetration length of water molecules into unstrained glass should be approximately 3 pm (respectively 0.3 Å) during the time it takes for a crack moving at 10^{-6} m s^{-1} (respectively at 10^{-8} m s^{-1}) to cover 100 μm.

However, because of the huge stresses concentrated at the crack tip, diffusion is enhanced by orders of magnitude in the vicinity of the tip during fracture [33,34], as observed in several other materials [35,36]. Therefore, water is expected to penetrate into the glass and, because of the heterogeneity of the material mentioned above, starts breaking bonds and create microcracks ahead of the crack tip. This in turn increases further the diffusion of water, thereby creating more corrosion and potentially leading to a substantial damaged zone. If this scenario is correct, a rather thick layer of water should remain trapped underneath the nominal fracture surface after the crack has propagated and stresses have relaxed. Since the diffusion constant is so small in unloaded silica glass (more than 100 days for traveling 1 nm), one should observe post-mortem a "fossil" water profile, essentially frozen-in at the time of its creation, with a thickness of the order of the size of the damaged zone.

Fracture was conducted, as in the previous series of experiments, on DCDC samples (Fig. 3) made of Corning 7980 pure silica. It was performed in a glove box that had been saturated with heavy water. After having initiated the two cracks, we have adjusted the load in order to reach the desired velocity [13]. Zone 1 (Fig. 6c) corresponds to an average velocity of 10^{-8} m s^{-1}. Zone 2 (Fig. 6c) corresponds an average velocity of 10^{-6} m s^{-1}.

Interaction potentials between a neutron and the nucleus of a given atom are proportional to the so-called "coherent length density" b. If b is positive, the interaction potential is attractive, while if b is negative, it is repulsive. One can show

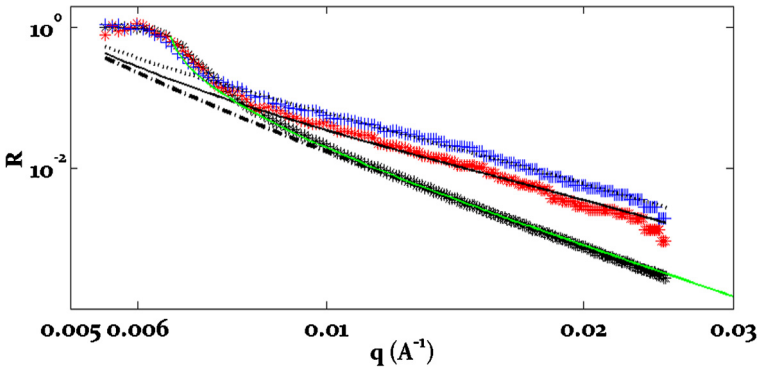

Fig. 7. (Color online.) Reflectivity as a function of scattering vector q: ⋆ control sample; ⋆ Zone 1, crack velocity $v = 4 \cdot 10^{-9}$ m s^{-1}; + Zone 2, crack velocity $v = 10^{-6}$ m s^{-1}. The green solid line (—) is not a fit, but it corresponds to the exact expression of the Fresnel reflectivity (Eq. (2)). The black dashed-dotted line is the result of the second Born approximation applied to the case of the pure silica diopter. One can see that it is a very bad approximation close to the Brewster conditions for total reflectivity, but that it becomes quite accurate for large values of q (in fact for $q > 0.01$ Å^{-1}). Fits in solid and dotted black lines of the reflectivities by zones 1 and 2, respectively, correspond to Eqs. (12) and (13), with $\phi_0^{\mathrm{I}} = 0.348 \pm 0.003$, $\ell^{\mathrm{I}} \approx 43$ Å and $\Lambda^{\mathrm{I}} \approx 35$ Å in (slow) Zone 1, while in (fast) Zone 2, $\phi_0^{\mathrm{II}} = 0.567 \pm 0.003$, $\ell^{\mathrm{II}} \approx 46$ Å and $\Lambda^{\mathrm{II}} \approx 23$ Å.

that the refraction index of the material is larger than unity if b is negative, and smaller than unity if b is positive. Although neutron refractive indices are always quite close to unity, a large, positive value of b may lead to a significant increase in reflectivity. Heavy water has been chosen because its coherent length density ($b_{\mathrm{w}} = 6.39 \cdot 10^{-6}$ Å^{-2}) is higher than the one of silica ($b_{\mathrm{s}} = 3.41 \cdot 10^{-6}$ Å^{-2}), and of opposite sign to that of light water ($-0.53 \cdot 10^{-6}$ Å^{-2}). If some water is trapped in the vicinity of the surface of the sample, the reflectivity of the sample should thus increase in the presence of heavy water, whereas it should weakly decrease with light water.

Specular Neutron Reflectivity (SNR) measurements have been carried out on the horizontal time-of-flight EROS reflectometer (CEA-Saclay, France) with a fixed angle θ of 1.195 degree, with a neutron white beam covering wavelengths λ from 4 Å to 25 Å, covering an accessible range of diffusion vectors $q = 2\pi \sin\theta/\lambda$ from 0.005 Å^{-1} to 0.032 Å^{-1}.

Zones 1 and 2 (see Fig. 6c) described above were studied. In order to select one of these areas of interest, we used the following trick. The sample was almost completely hidden on the neutrons path by two black sheets of B_4C, a strong neutron absorber, to let the neutrons illuminate only the desired region (Fig. 6a and b). In order to test that the selected region was flat enough to allow a correct measurement, we have checked that the half full width of the alignment rocking curve was lower than 0.025°. When this was not the case, the illuminated region was reduced until this condition was met. The resulting illuminated surfaces were very small, of the order of ∼25 mm^2. Because of this smallness, we used very long counting times to get a reasonable noise-to-signal ratio, up to 48 h per illuminated region. In particular, we measured the background independently of the sample with great precision, enabling its subtraction with a good accuracy.

The experimental curves presented in Fig. 7 clearly show a huge change in the reflectivity of broken samples when compared to the reflectivity of an unbroken control specimen. Since the roughness of the fracture surfaces is larger than the roughness of the control specimen, one should *a priori* expect a decrease of the reflectivity of the broken samples. The difference seen in Fig. 7 is therefore underestimated. In addition, let us note that the effect of the crack growth velocity on the reflectivity should reveal the important role played by failure mechanisms on the concentration of water close to the fracture surface. Indeed, crack velocity governs both the level of stress in the zone close to the tip and the diffusion time.

Fig. 7 shows also that the reflectivity of the control specimen corresponds perfectly to the Fresnel reflectivity

$$R_{\mathrm{F}} = \left(q - \sqrt{\left(q^2 - 4\pi N b_{\mathrm{g}}^0\right)}\right)^2 / \left(q + \sqrt{\left(q^2 - 4\pi N b_{\mathrm{g}}^0\right)}\right)^2 \tag{2}$$

of a semi-infinite silica diopter for which the coherent length density is equal to $N b_{\mathrm{g}}^0 = 3.41 \cdot 10^{-6}$ Å^{-2} [37,38]. Eq. (2) is plotted in green in Fig. 7.

Our fit of the data is based on the observation that neutron transmission coefficients are usually close to unity (except in the vicinity of the Brewster incidence angle). The basic assumption of our approximate calculation is thus that even a silica diopter is a perturbation of the free case.

Let us call $\phi(z)$ the heavy water volume fraction at a distance z from the surface.

The neutron wave function ψ obeys the following eigenvalue equation:

$$\frac{\mathrm{d}^2\psi(z)}{\mathrm{d}z^2} + \left(q^2 - V(z)\right)\psi(z) = 0 \tag{3}$$

where $V(z) = 0$ corresponds to the free case, and $V(z) = 4\pi\left(b_{\mathrm{s}} + b_{\mathrm{w}}\phi(z)\right)$ is a small perturbation: $V(z) \ll q^2$. In the absence of heavy water, the perturbative term is simply $V(z) = 4\pi b_{\mathrm{s}}$.

We write:

$$\psi = \psi_0 + \psi_1 + \psi_2 + \ldots \tag{4}$$

with ψ_1 and ψ_2 the first- and second-order corrections (in V).

Adapting the calculation of [39], one finds:

$$\psi_{n+1}(z) = \int_0^\infty \mathrm{d}z' V(z') \psi_n(z') G_0(z, z') \tag{5}$$

where the Green function G_0 $(z, z' > 0)$, relevant for our boundary conditions, refers to the free case:

$$G_0(z, z') = -\frac{1}{2\mathrm{i}q} \exp\bigl(-\mathrm{i}q(z' - z)\bigr) \quad \text{if } z < 0$$
$$G_0(z, z') = -\frac{1}{2\mathrm{i}q} \exp\bigl(-\mathrm{i}q|z' - z|\bigr) \quad \text{if } z > 0 \tag{6}$$

Hence:

$$\psi_1(z) = \frac{\mathrm{i}}{2q}\left[\int_0^z \mathrm{d}z' V(z') \exp(-\mathrm{i}qz) + \int_z^\infty \mathrm{d}z' V(z') \exp\bigl(-2\mathrm{i}qz'\bigr) \exp(\mathrm{i}qz)\right] \tag{7}$$

and:

$$\psi_2(z) = \int_0^\infty \mathrm{d}z' V(z') \psi_1(z') G_0(z', z) \tag{8}$$

with $z' > 0$ and $z < 0$.

Adding the first- and second-order contributions, we get the expression of the reflectance r to order V^2:

$$r = \frac{\mathrm{i}}{2q} \int_0^\infty \mathrm{d}z' V(z') \, \mathrm{e}^{-2\mathrm{i}qz'} - \frac{1}{4q^2} \int_0^\infty \mathrm{d}z' V(z') \tag{9}$$

$$\times \left[\mathrm{e}^{-2\mathrm{i}qz'} \int_0^{z'} \mathrm{d}z'' V(z'') + \int_{z'}^\infty \mathrm{d}z'' V(z'') \, \mathrm{e}^{-2\mathrm{i}qz''}\right] \tag{10}$$

The reflectivity R is equal to $R = |r|^2$.

In order to check the validity of our second-order Born approximation, we first verify that our result in Eq. (10) tends to the Fresnel reflectivity for high values of q when V is a constant equal to $q_c^2 = 4\pi b_s$. This limit leads to the following reflectivity:

$$R = r_0^2 = \frac{q_c^4}{16q^4}\left(1 + \frac{q_c^2}{2q^2}\right)^2 + O\left(\frac{q_c^8}{q^8}\right) \tag{11}$$

which coincides with the corresponding large q expansion of the Fresnel reflectivity.

We then tried to fit the reflectivities in zones 1 and 2 (Fig. 7) using the simplest function involving a single length scale, i.e. $\phi(z) = \phi_0 \exp(-z/\Lambda)$. Although this can be made to fit the Zone 1 results, the reflectivity increase in Zone 2 is too large to be accounted for by using this simple function. Hence, guided by the idea that there might be a saturated layer of depth ℓ close to the surface that becomes more diffuse deeper in the sample, we posit that:

$$\phi_w(z) = \phi_0 \quad \text{if } z < \ell$$
$$\phi_w(z) = \phi_0 \exp\bigl(-(z - \ell)/\Lambda\bigr) \quad \text{if } z > \ell \tag{12}$$

This choice leads to a reflectance r that can be written as: $r = r_0 + r_1 + r_2$, with r_0 as the Fresnel reflectance (Eq. (11)) and:

$$r_1 = -\frac{2\pi b_w \phi_0}{q(2\mathrm{i}q\Lambda + 1)} \exp(-2\mathrm{i}q\ell) \tag{13}$$

$$r_2 = -\frac{4\pi^2 (b_w \phi_0)^2}{q^2}\left[\frac{1}{2q^2}\bigl[\exp(-2\mathrm{i}q\ell)(1 + 2\mathrm{i}q\ell) - 1\bigr] + \frac{\Lambda \exp(-2\mathrm{i}q\ell)}{(2\mathrm{i}q\Lambda + 1)(\mathrm{i}q\Lambda + 1)}(\Lambda + 2\ell + 2\mathrm{i}q\Lambda\ell)\right] \tag{14}$$

Fig. 7 shows the best fits of the experimental measurements performed on the two fracture surfaces using Eqs. (11), (13) and (14):

$$R = |r_0 + r_1 + r_2|^2 \tag{15}$$

The best fit is achieved with $\phi_0^{\mathrm{I}} = 0.348 \pm 0.003$, $\ell^{\mathrm{I}} \approx 43$ Å and $\Lambda^{\mathrm{I}} \approx 35$ Å in (slow) Zone 1, while in (fast) Zone 2, $\phi_0^{\mathrm{II}} = 0.567 \pm 0.003$, $\ell^{\mathrm{II}} \approx 46$ Å and $\Lambda^{\mathrm{II}} \approx 23$ Å. Note that ϕ_0 is very accurately determined by the fit, although the error bar we quote only accounts for statistical uncertainty, and not systematic effects coming from the choice of the fitting function and of the interval over which the data is fitted. On the other hand, the quality of fit has a "soft direction" in the plane (ℓ, Λ). In other words, the total effective width of the layer, $\ell_{\mathrm{eff}} = \ell + \Lambda$, is better determined than ℓ and Λ separately. The statistical error bar on ℓ_{eff} is smaller than 1 Å, but again systematic errors are larger.

5. Discussion

Molecular mechanisms accompanying crack propagation in glass in a humid environment are still ill-understood, for an obvious reasons: they concern length scales that can hardly been reached directly. Hence, only indirect evidences can be invoked to make progress in the understanding of molecular-scale mechanisms involved in the stress corrosion fracture of silica, and, more generally, of amorphous materials.

In this paper, we have shown three different indirect proofs that (i) water penetrates into glass during fracture, and that (ii) the presence of water induces damage spreading through Si–O bond breaks due to local hydrolysis.

Indeed, we have shown, by measuring neutron reflectivity, that water is stored under fracture surfaces. This means that water penetrates into glass during fracture over distances of $\Lambda \simeq 10$ nm. Once water has penetrated into silica, we know that there is a given probability, depending on the humidity rate, that an Si–O bond is broken. This leads to the formation of a damaged zone, the extent of which depends on crack velocity.

The signature of the existence of a damaged zone can be seen in the morphology of fracture surfaces. Indeed, over length scales which are of the order of 10 to 20 nm, the morphology of glass fracture surfaces is similar to the one of materials as different as metallic alloys, mortar, wood, etc. when observed within their damaged zone.

Furthermore, the signature of damage preceding a stress corrosion crack was also observed directly with AFM in several silica-based glasses.

These are all indirect proofs, and in most cases—except, probably, neutron reflectivity—, experimental techniques are pushed close to the limits of their resolutions. However, put together, they constitute a coherent body of evidences that converge to the following scenario: due to huge strains in the vicinity of a crack tip, water penetrates into glass during crack propagation, and hydrolyses Si–O bonds. The "nanocracks" formed tend to grow under local loading, and water penetrates even more because of the presence of this damage.

It is tempting to describe this mechanism in one dimension (along the direction x of crack propagation) by solving the following set of coupled equations:

$$\begin{aligned} &V\phi(x) + D(x)\frac{\partial \phi(x)}{\partial x} = V_0\phi_0 \\ &D(x) = D_0 \exp\left(\frac{\delta(x)}{\delta_0}\right) \\ &V\frac{\mathrm{d}\delta(x)}{\mathrm{d}x} = -\frac{\phi(x)}{\tau}F\big(\sigma(x)\big) \end{aligned} \tag{16}$$

where $D(x)$ is the diffusion coefficient at a distance x from the crack tip, $\delta(x)$ is a damage variable (equal to unity when there is no material located at x, equal to zero when the material is unbroken). The first of these equations is the diffusion equation written in the reference frame of the crack, which moves at velocity V. The second one expresses that $D(x)$ increases exponentially with damage, and the third one reflects the fact that damage depends both on the local stress $\sigma(x)$ (through a given function F) and on the local water volume fraction $\phi(x)$, but also that it depends on the crack velocity V. In fact, the last of this set of equations reflects the fact that the slower the crack, the more time damage has to spread. τ is a characteristic time needed to nucleate damage.

Unfortunately, the function F of local stress $\sigma(x)$ is not better known than constants $(V_0\phi_0)$ and τ. Because of the very structure of these equations, which have exponential-like solutions, it is hopeless to try solving them without performing more experiments where both humidity rate and crack velocity are controlled. Molecular Dynamics coupled to *ab initio* simulations, whenever they can be performed on large-enough samples, will be very useful in understanding the complex mechanisms of stress corrosion.

Acknowledgements

The author wishes to thank all her collaborators on the topic of glass stress corrosion: J.-P. Bouchaud, F. Célarié, S. Chapuliot, F. Cousin, C. Guillot, F. Lechenault, C. Marlière, L. Ponson, S. Prades, K. Ravi-Chandar, and C.-L. Rountree.

References

[1] A.A. Griffith, The phenomena of rupture and flow in solids, Philos. Trans. R. Soc. Lond. A 221 (1921) 163–198.
[2] B. Lawn, Fracture of Brittle Solids, Second Edition, Cambridge University Press, 1993.
[3] R.T. Sanderson, Chemical Bonds and Bond Energy, Academic Press, 1971.
[4] F. Célarié, S. Prades, D. Bonamy, L. Ferrero, A. Dickelé, É. Bouchaud, C. Guillot, C. Marlière, Surface fracture of glassy materials as detected by real-time atomic force microscopy experiments, Appl. Surf. Lett. 212–213 (2003) 92–96.
[5] D. Bonamy, É. Bouchaud, Failure of heterogeneous materials: a dynamic phase transition? Phys. Rep. 498 (2011) 1–44.
[6] A. Nakano, R.K. Kalia, P. Vashishta, Dynamics and morphology of brittle cracks: a molecular-dynamics study of silicon-nitride, Phys. Rev. Lett. 75 (1995) 3138–3141.
[7] P. Guan, S. Lu, M.J.B. Spector, P.K. Valavala, M. Falk, Cavitation in amorphous solids, Phys. Rev. Lett. 110 (2013) 185502.
[8] C.L. Rountree, R.K. Kalia, E. Lidorikis, A. Nakano, L. Van Brutzel, P. Vashishta, Atomistic aspects of crack propagation in brittle materials: multimillion atom molecular dynamics simulations, Annu. Rev. Mater. Res. 32 (2002) 377–400.
[9] M.L. Falk, Molecular-dynamics study of ductile and brittle fracture in model noncrystalline solids, Phys. Rev. B 60 (1999) 7062–7070.
[10] P. Daguier, S. Hénaux, É. Bouchaud, F. Creuzet, Quantitative analysis of a fracture surface by atomic force microscopy, Phys. Rev. E 53 (1996) 5637.
[11] F. Célarié, S. Prades, D. Bonamy, L. Ferrero, É. Bouchaud, C. Guillot, C. Marlière, Glass breaks like metals, but at the nanometer scale, Phys. Rev. Lett. 90 (2003) 075504.
[12] C. Marlière, S. Prades, F. Célarié, D. Dalmas, D. Bonamy, L. Ferrero, A. Dickelé, C. Guillot, É. Bouchaud, Crack fronts and damage in glass at the nanometer scale, J. Phys. Condens. Matter 15 (2003) S2377–S2386.
[13] S. Prades, D. Bonamy, D. Dalmas, É. Bouchaud, C. Guillot, Nano-ductile propagation in glasses under stress corrosion: spatio-temporal evolution of damage in the vicinity of the crack tip, Int. J. Solids Struct. 42 (2004) 637–645.
[14] S.M. Wiederhorn, Moisture assisted crack growth in ceramics, Int. J. Fract. Mech. 4 (1968) 171–177.
[15] S.M. Wiederhorn, Fracture surface energy of glass, J. Am. Ceram. Soc. 52 (1969).
[16] M. Ciccotti, Stress-corrosion mechanisms in silicate glasses, J. Phys. D, Appl. Phys. 42 (2009) 214006, Special Issue “Fracture: from the atomic to the geophysical scale”, Guest Editors É. Bouchaud and P. Soukiassian.
[17] T.A. Michalske, B.C. Bunker, Slow fracture model based on strained silicate structures, J. Appl. Phys. 56 (1984) 2686–2693.
[18] F. Lechenault, C.L. Rountree, F. Cousin, J.-P. Bouchaud, L. Ponson, É. Bouchaud, Evidence of deep water penetration into silica during stress corrosion fracture, Phys. Rev. Lett. 106 (2011) 165504.
[19] F. Lechenault, C.L. Rountree, F. Cousin, J.-P. Bouchaud, L. Ponson, É Bouchaud, Damage of silicate glasses during stress corrosion, J. Phys. Conf. Series 319 (2011) 012005;
Continuum Models for Discrete Systems International Conference (CMDS 12), Kolkatta, India.
[20] B.B. Mandelbrot, D.E. Passoja, A.J. Paullay, Fractal character of fracture surfaces of metals, Nature 308 (1984) 721–722.
[21] É. Bouchaud, G. Lapasset, J. Planes, Fractal dimension of fractured surfaces: a universal value? Europhys. Lett. 13 (1990) 73.
[22] L. Ponson, D. Bonamy, É. Bouchaud, Two dimensional scaling properties of experimental fracture surfaces, Phys. Rev. Lett. 96 (2006) 035506.
[23] L. Ponson, Crack propagation in disordered materials: how to decipher fracture surfaces, Ann. Phys. 32 (1) (2007).
[24] F. Célarié, M. Ciccotti, C. Marlière, Stress-enhanced ion diffusion at the vicinity of a crack tip as evidenced by atomic force microscopy in silicate glasses, J. Non-Cryst. Solids 353 (2007) 51–68.
[25] F. Lechenault, G. Pallares, M. George, C. Rountree, É. Bouchaud, M. Ciccotti, Effects of finite probe size on self-affine roughness measurements, Phys. Rev. Lett. 104 (2010) 025502.
[26] M.Y. He, M.R. Turner, A.G. Evans, Analysis of the double cleavage drilled compression specimen for interface fracture energy measurements over a range of mode mixities, Acta Metall. Mater. 43 (1995) 3453–3458.
[27] J.-P. Guin, S.M. Wiederhorn, Fracture of silicate glasses: ductile or brittle? Phys. Rev. Lett. 92 (2004) 215502.
[28] J.M. Lòpez-Cepero, S.M. Wiederhorn, T. Fett, J.-P. Guin, Do plastic zones form at crack tips in silicate glasses? Int. J. Mater. Res. 98 (2007) 1170–1176.
[29] K. Han, M. Ciccotti, S. Roux, Measuring nanoscale stress intensity factors with an atomic force microscope, Europhys. Lett. 89 (2010) 66003.
[30] K.M. Davis, M. Tomozawa, An infrared spectroscopic study of water-related species in silica glasses, J. Non-Cryst. Solids 201 (1996) 177–198.
[31] S. Berger, M. Tomozawa, Water diffusion into a silica glass optical fiber, J. Non-Cryst. Solids 324 (2003) 256–263.
[32] M. Tomozawa, K.M. Davis, Time dependent diffusion coefficient of water into silica glass at low temperatures, Mater. Sci. Eng. A 272 (1999) 114–119.
[33] F.C. Larché, P.W. Voorhees, Diffusion and stresses: basic thermodynamics, Defect Diffus. Forum 129 (130) (1996) 31–36.
[34] H. Mehrer, The effect of pressure on diffusion, Defects Diffusion Forum 129 (130) (1996) 57–76.
[35] M.J. Aziz, Y. Zhao, H.-J. Gossmann, S. Mitha, S.P. Smith, D. Schiferl, Pressure and stress effects on the diffusion of B and Sb in Si and Si–Ge alloys, Phys. Rev. B 73 (2006) 054101.
[36] J. Guery, J. Baudry, D.A. Weitz, P.M. Chaikin, J. Bibette, Diffusion through colloidal shells under stress, Phys. Rev. E 79 (2009) 060402.
[37] F. Cousin, A. Menelle, La réflectivité de neutrons, in: A. Ayral, V. Rouessac (Eds.), Techniques Innovantes pour la Caractérisation Optique Microstructurale de Couches Minces, in: Sciences et Techniques de l'Ingénieur, CNRS Éditions, Paris, 2006.
[38] http://www.sfn.asso.fr/Enseignement/Outils/Table/index.html.
[39] J.-C. Charmet, P.-G. de Gennes, Ellipsometric formulas for an inhomogeneous layer with arbitrary refractive index profile, J. Opt. Soc. Am. 73 (1983) 1777–1784.